Int. J. Electrochem. Sci., 11 **(2016)** 4389 – 4398, doi: 10.20964/2016.06.12

International Journal of
ELECTROCHEMICAL
SCIENCE
www.electrochemsci.org

A Facile Hydrothermal Synthesis of Ultrasmall Sn Nanoparticles in Carbon Matrices as Anode for Lithium Ion Battery

Jie Qu[1,2], *YonganYang*[2,*] , *ZhihuiChen*[2], *YurongRen*[1], *JianningDing*[1,*], *NingyiYuan*[1]

[1] School of Materials Science and Engineering, Jiangsu Collaborative Innovation Center of Photovoltaic Science and Engineering and Jiangsu Province Cultivation base for State Key Laboratory of Photovoltaic Science and Technology, Changzhou University, Changzhou 213164, P. R. China
[2] Department of Chemistry and Geochemistry, Colorado School of Mines, 1012 14th Street, Golden, CO, 80401, U.S.A
[*]E-mail: dingjn@cczu.edu.cn, Yongan@mines.edu

Received: 29 February 2016 / *Accepted:* 23 March 2016 / *Published:* 4 May 2016

Ultrasmall sub-5nm nanoparticles in carbon matrices are synthesized by a facile hydrothermal route. The morphology and structure of the prepared samples were characterized by transmission electron microscopy (TEM) and X-ray diffraction (XRD). The electrochemical performances were evaluated by galvanostatic cycling and cyclic voltammetry. It is found that among the three nanocomposites Sn/C-3 with Sn nanoparticles content of 20.9wt% shows the best rate performance and the highest discharge capacity. At the current density of 200 mA g^{-1}, it shows a high dicharge capacity of 851.8 mAh g^{-1}. Even when the current density is increased to 5000 mA g^{-1}, a high discharge capacity of 168.1 mAh g^{-1} can still be obtained. This result indicates a potential suitability of fabricating Sn/C electrode with high electrochemical performance.

Keywords: ultrasmall Sn; carbon; hydrothermal synthesis; lithum-ion battery

1. INTRODUCTION

Lithium-ion batteries due to their high energy density, improved rate capability and flexibility are widely used as the main power sources for portable electronics and have a promising application in future transportation and large-scale energy storage [1-3]. Currently, carbonaceous materials such as graphite are commercial anodes due to their low potential plateau, good capacity, and low costs. However, the theoretical capacity of graphite anode is low, only 372 mAh g^{-1} [4], not meeting the

future need. Thus, tremendous efforts have been done on the improvement of carbonaceous anode and development of new anode [5-7].

As one of the most promising candidates to displace commercialized graphite, the operating potential of metallic Sn is slightly higher than graphite [8-10], and the extrapolating potential is close to Li to improve the safety of LIBs [11]. Also Sn can be reversibly lithiated up to the end compound $Li_{4.4}Sn$ with a theoretical reversible capacity of 994 mAh g^{-1}, almost three times higher than the theoretical value of the conventional graphite anode [12-15]. However, the practical use of Sn anodes has been hindered by the short cycle life due to a large volume expansion of Sn during lithiation-delithiation process [16-17]. Almost 300% of its initial volume expansion would result in serious mechanical stress causing rapid crackingand collapse of the structure, and loose contact between the anode and the current collector, thereby drastic capacity fading [18-19].

Enormous efforts have been devoted to improve the electrochemical performance of metallic Sn [11,16,20]. Reducing the particle size have been considered as an efficient method, which can mitigate the mechanical stress induced by the large volume expansion during lithiation-delithiation process, and prevent particle pulverization [21-23]. Nevertheless, the small size would enable the nanoparticles aggregation, resulting in the inevitable capacity decay [21,24]. To integrate Sn with a conductive matrix such as carbon, is an attractive method to resolve the above problems. A carbonaceous matrix here can increase the electrical conductivity of the anode, and present abuffering effect to accommodate the volume expansion during lithiation-delithiation process. Furthermore, it can also prevent the aggregation of Sn nanoparticles, thus improving the cyclability of Sn-based electrodes [25-26].

Many methods have been used to synthesize Sn-carbon composites, such as ball milling [27-28], chemical vapor deposition (CVD) [29], solid-state reaction [30] and microwave plasma chemical vapor deposition [31-33]. However, most of the methods are high costs or complicated. In addition, Sn particles could fall off carbon during the charge-discharge process. Thus, facile approaches are worth exploring to improve the adhesion of Sn on C forhigh-performance Sn-carbon composites.

In this work, we report a one-step method of synthesizing of Sn/C nanocomposites with low cost of the precursors. Sn nanoparticles are only 5-10 nm, and adhere to carbon strongly. A preliminary investigation on the electrochemical properties of theas-prepared samples was carried out.

2. EXPERIMENTS

Tin precursor solution was prepared by dissolving $SnCl_4$ (chemical, 2.6 g) in ethanol (20 mL). NaOH precursor solution was prepared by dissolving NaOH (9.6 g) in water (60 mL).

2.1. Synthesis of four morphologies of **Sn/C** *nanomaterials*

Sn/C-1: glucose (9.6 g) was added to NaOH precursor solution. After stirring and sonicating for several minutes, a clear solution was obtained. Then tin precursor solution (1 ml) was added

dropwise to the above solution under stirring for 1h. The resultant solution was transferred into a Teflon-lined autoclave (100 mL) and treated at 180 ˚C for 4 h. The product was recovered and rinsed with distilled water, then ethanol. After being dried at 60 ˚C for about 24h, the as-prepared sample was calcined in an oven at 700 ˚C for 2h under Ar atmosphere.

Sn/C-2: The synthesis process was similar to **Sn-C-1** with the tin precursor solution changed to 2 ml.

Sn/C-3: The synthesis process was similar to **Sn-C-1** with the tin precursor solution changed to 4 ml.

2.2. Structural analysis

The characterization of the as-prepared samples was carried out by X-ray diffraction (XRD, D/max 2500 PC), thermal gravimetric analysis (TGA, SDT Q600) under Oxygenwith a rate of 10 ^{o}C /min, fourier transform infrared (FTIR, BIO-RAD FTS6000) spectroscopy and transmission electron microscopy (TEM, FEI TecnaiG20). N_2 adsorption data was measured using a NOVA 2000e (Quantachrome) instrument, while the specific surface area was evaluated by the BET method.

2.3. Preparation of the electrodes and electrochemical methods

The electrochemical properties were measured using two-electrode cells with electrodes prepared using mixtures comprising of 75％active material, 18％Acetylene Black and 7％ PVDF (Polyvinylidene Fluoride), pressed into pellets. Lithium metal was used as the counter and reference electrode. The electrolyte was $LiPF_6$ (1 M) in a mixture of ethylene carbonate (EC) and diethyl carbonate (DEC) at a weight ratio of 1:1. The galvanostatic method at the discharge-charge current density of 200 mAg^{-1}, 500 mAg^{-1}, 1000 mAg^{-1}, 2000 mAg^{-1} and 5000 mAg^{-1} was used to measure the electrochemical capacity of the electrodes at room temperature using a MTI-BST8-MA(10 mA). The cutoff potentials for charge and discharge were set at 3.0 and 0.01 V vs Li^{+}/Li, respectively. The CV experiments were conducted using GAMRY REFERENCE 600 at room temperature.

3. RESULTS AND DISCUSSION

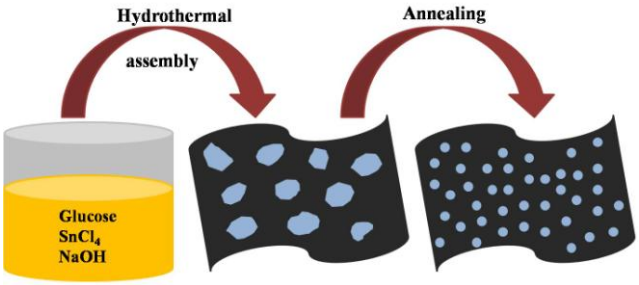

Figure 1. Schematic illustration of the synthesis route to Sn/C nanocomposites.

Fig. 1 shows the synthesis route of the samples. Through hydrothermal method, using the same original materials, changing the tin precursor solution to 1 ml, 2 ml and 4 ml, after annealing at 700°C for 2h under argon, Sn/C nanocomposites with different Sn content are prepared.

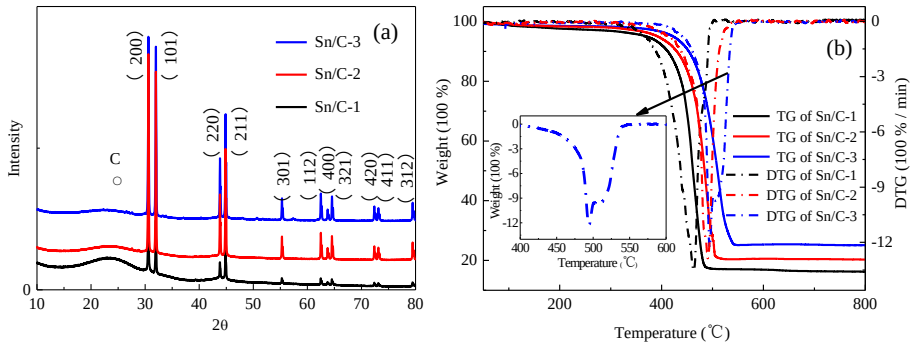

Figure 2. XRD patterns (a) and TG and DTG curves (b) of the three samples.

Fig. 2a is the XRD patterns of as-prepared Sn/C samples. All thesamples show the characteristic peaks of the tetragonal tin metal (JCPDS#04-0673). And an additional weakened and broadenedpeak at about 25º due to the diffraction of the carbon (JCPDS#75-2078), suggesting an amorphous or poorly crystalline character [33]. The thermal behaviors of the three compositesare investigated by thermalgravimetric analysis (TGA) as shown in Fig. 2b. Asreported previously, the little weight lossobserved until about 280 ˚C in the TG curve is attributed to the elimination of adsorbed water and air [11]. Astrong weight loss between the 400-600˚C for all of the three samples are observed correlating with a strong exothermic peak at 463 ˚C for Sn/C-1 and 490.8 ˚C for Sn/C-2 in DTG curves, which maybe related to a mixed oxidation of carbon and tin. However, two exothermic peaks are observed for Sn/C-3, a strong peak appeared at 494.3 may relate to the oxidation of carbon and a weak peak at 505.5 may relate to oxidation of tin. At the temperature of 700 ˚C all carbon and tin in the composites are converted to CO_2 and SnO_2, respectively. Thus, the remaining weight is the weight of SnO_2. The Sn content in the composite can be estimated from the amount of SnO_2. The Sn contents of all the prepared composites are 13.2% forSn/C-1, 16.7% for Sn/C-2 and 20.9% for Sn/C-3. The nitrogen absorption test was also applied to the three samples. The BET surface area is 146.3, 172.5, 196.8 m^2/g for Sn/C-1, Sn-C/2 and Sn/C-3, respectively.

Fig. 3 shows the TEM images of the as-prepared Sn/C samples. It can be clearly seen that the Sn nanoparticles with an average particle size of about 5-6 nm are dispersed onto the thick carbon layers. The uniform distribution of Sn nanoparticles on carbon may due to the one step synthesis. And the appropriate and lower concentration ofthe precursor solution coupled with the stable carbon layers can effectively prevent Sn nano-grains from growing bigger. The crystal lattice fringes of tin particles are clearly detected and the average distance between adjacent lattice planes is 0.29 nm, corresponding to the (200) plane of crystalline Sn (JCPDS no. 04-0673).

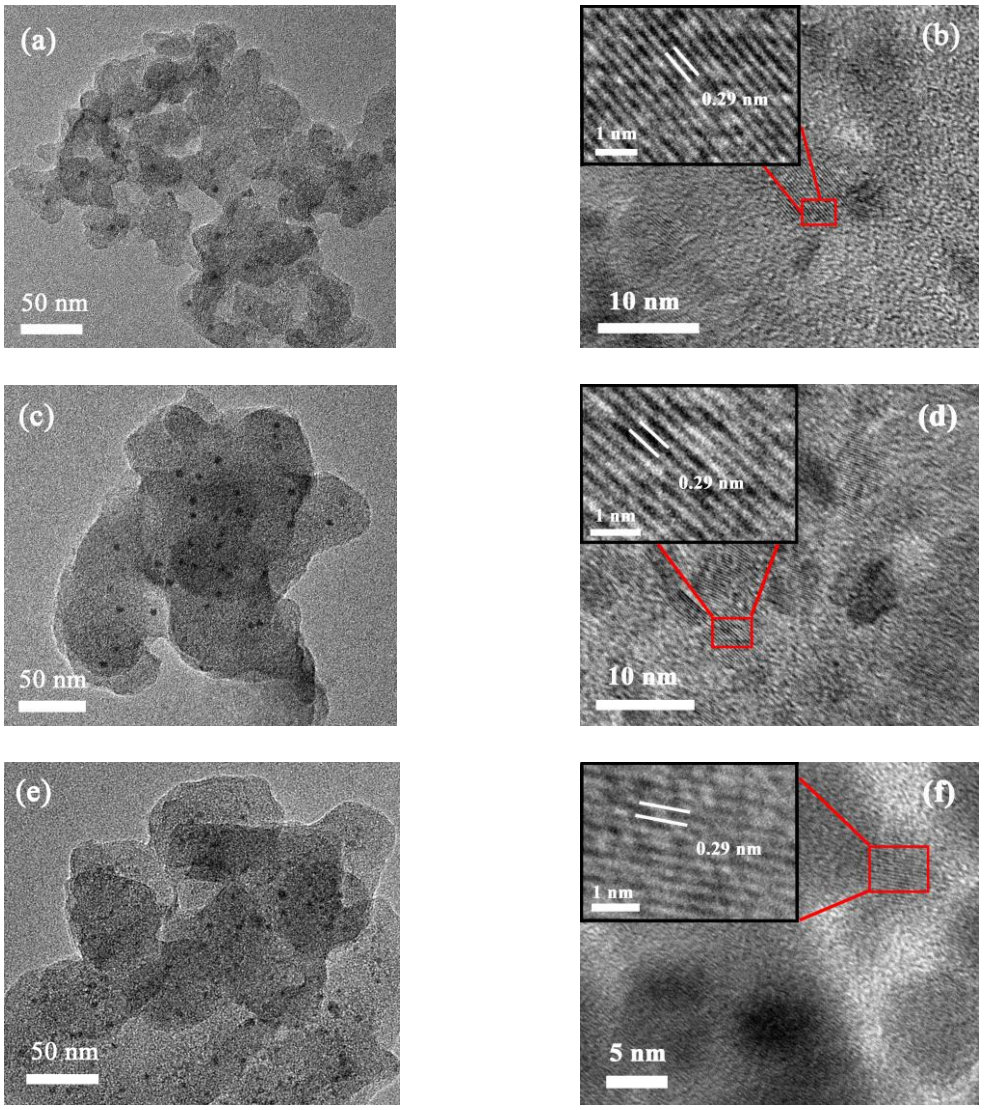

Figure 3. Typical TEM images of Sn/C-1 (a, b), Sn/C-2 (c, d) and Sn/C-3 (e, f).

The nature of the Sn/C nanocomposites was studied by infrared spectroscopy as shown in Fig. 4a. It is clear that the band around 3400 cm^{-1} is indicated to O-H stretching vibration of water, while the band around 1600 cm^{-1} is indicated to C=C stretching. Two weak bands at about 1380 and 1180 can be corresponded to C-O stretching. There is also a weak band around 560 cm^{-1} which can be indicated to the Sn-OH terminal bonds stretching [34-36]. Such hydrophilic characteristics can make Sn nanoparticles easily, uniformly and stably dispersed on the carbon sheet.

The wide survey XPS spectra of three Sn/C samplesare showed in Fig. 4b, which reveals the presence of C, O and Sn elements. The peaks at 496.1 and487.7 eV in Fig 4c can be assigned to the binding energy of Sn $3d_{3/2}$ andSn $3d_{5/2}$ respectively, which may indicate that the Sn existedhere is Sn^{4+} oxidation state rather than Sn^0 state. As reported previously, Sn nanoparticles in surface layer could possibly be oxidized in air during analysis, which can be observed in the XPS analysis of Sn nanoparticles [35,36]. The C 1s spectrum of carbon displays a strong peak at 284.8 and a weak peak at 289.9 eV, corresponding to C-C and O=C-O groups, respectively.

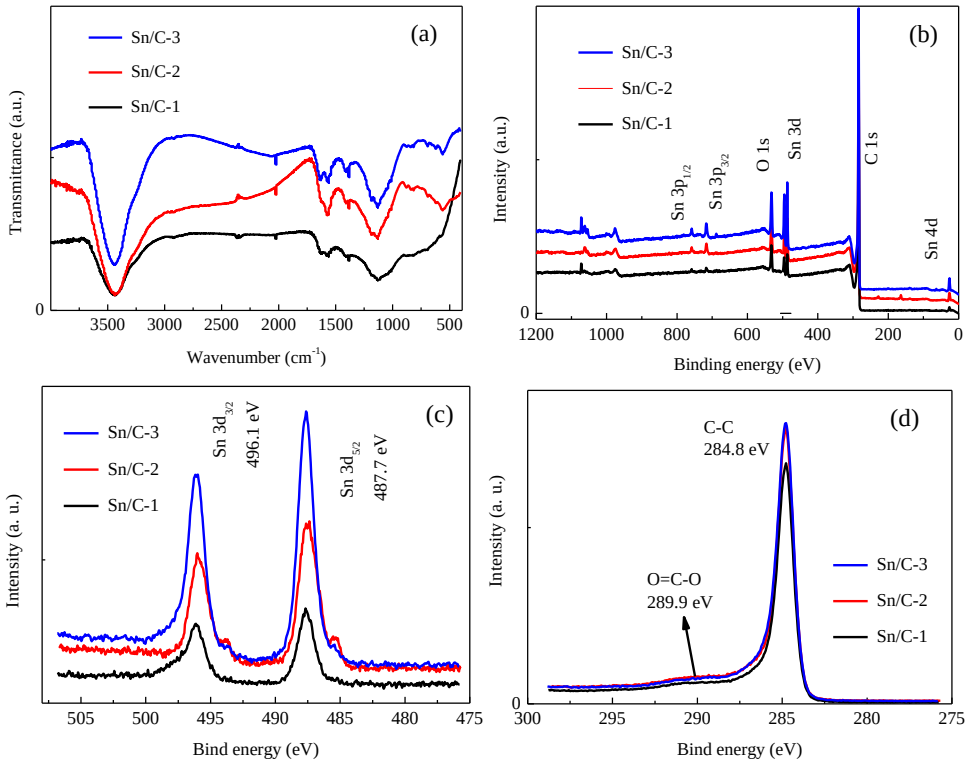

Figure 4. FTIR spectra (a) and XPS spectrum (b, c, d) of the three samples.

Fig. 5 shows the initial charge-discharge curves of the three composites at a current density of 200 mA g^{-1} between 0.01 Vand 3.0 V. The initial discharge and charge capacities are about 506.4 and 263.2 mAh g^{-1} for Sn/C-1, 712.3 and 332.1 mAh g^{-1} for Sn/C-2, and 851.8 and 355.1 mAh g^{-1} for Sn/C-3, respectively. The low coulombic efficiencies for all of the three samples in the first cycle can beassigned to the generation of SEI film on the electrode surface during the first discharge process and the irreversible Li trapped sites [18,28].

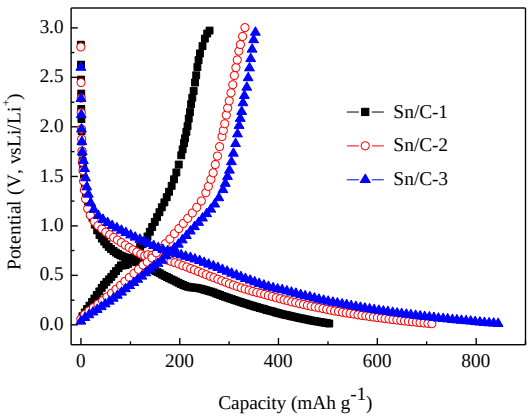

Figure 5. Initial discharge-charge curves of as-prepared samples at the current density of 50 mA g^{-1}.

To examine the high rate capability and cycle stability of the as-prepared samples, the discharge capacity at different current densities was determined (Fig.6). Sn/C-3 shows the highest discharge-charge capacities, then the Sn/C-2 and Sn/C-1. All of the samples show superior high rate performance. A discharge capacity of about 301.8 mAh g^{-1} for Sn/C-3 was obtained after the 20th cycle at the low current density of 200 mA g^{-1}. When the current density is increased to 5000 mA g^{-1}, the discharge capacity can still retained 168.1 mAh g^{-1} after 60 cycles. More importantly, after 60 cycles at varied current densities, Sn/C-3 still have the discharge capacity of 297 mAh g^{-1} at the current density of 200 mA g^{-1}, almost identical to the value in the 20th cycle. For Sn/C-2 and Sn/C-1, the discharge capacities are 243.7 and 180.3 mAh g^{-1} at the current density of 200 mA g^{-1} after 20th cycle, and 100.8 and 60.2 mAh g^{-1} at the current density of 5000 mA g^{-1} after 60 cycles. Compare the performance of our Sn/C-3 nanocomposite with the literature results (include Sn/graphene, Sn/CNTs and Sn/C nanocomposite) [37-40], it is found that our Sn/C-3 nanocomposite shows lower capacities at the low current density than Sn/graphene and Sn/CNTs, but comparative capacities at high current density with Sn/graphene and higher capacities than Sn/CNTs. Besides it shows much better performance than Sn/C nanocomposite. Therefore, Sn/C-3 can endure great changes of various low or high current densities to retain good stability upon cycling, which is a merit for high tolerance of lithium-ion batteries with the high power and long cycle life.

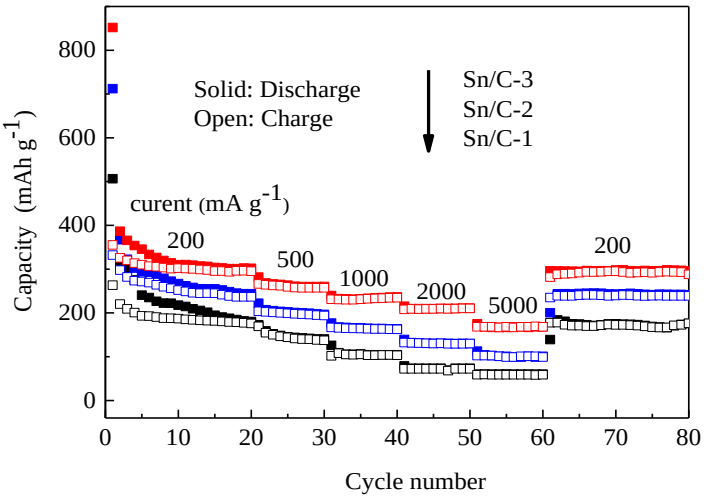

Figure 6. Cycle curves of as-prepared samples at different current densities.

A preliminary investigation on electrochemical properties is tested by the CV experiments at a scan rate of 0.1 mV s^{-1}. As shown in Fig. 7, in the first cycle, two broad cathodic peaks at approximately 0.36 V and 0.61 V were observed which can be attributed to the two-step lithiation of Sn with Li to form Li_xSn ($x \leq 4.4$) alloy [19, 41-42]. However in the second cycle, the cathodic peak at 0.61 V of Sn/C-2 and Sn/C-3 was almost disappeared, which maybe caused by the formation of a SEI layer [43]. Meanwhile, a current decrease between the first and the second cycle at the cathodic scanning is detected, which may be related to the irreversible intercalation of Li^+ ions in the carbon [44-45]. While four anodic peaks at approximately 0.46, 0.62, 0.73 and 0.80 V were observed, which can be assigned to delithiation of the Li_xSn alloy [46-48]. During the cycles, the four oxidation peaks

are quite stable, indicating a reversible deintercalation process of lithium ion from the Li_xSn alloy. Except the first cycle, all the peak current intensities were almost no change, implying a stable structure of the three Sn/C nanocomposites. This result can further vertify the cycle performance.

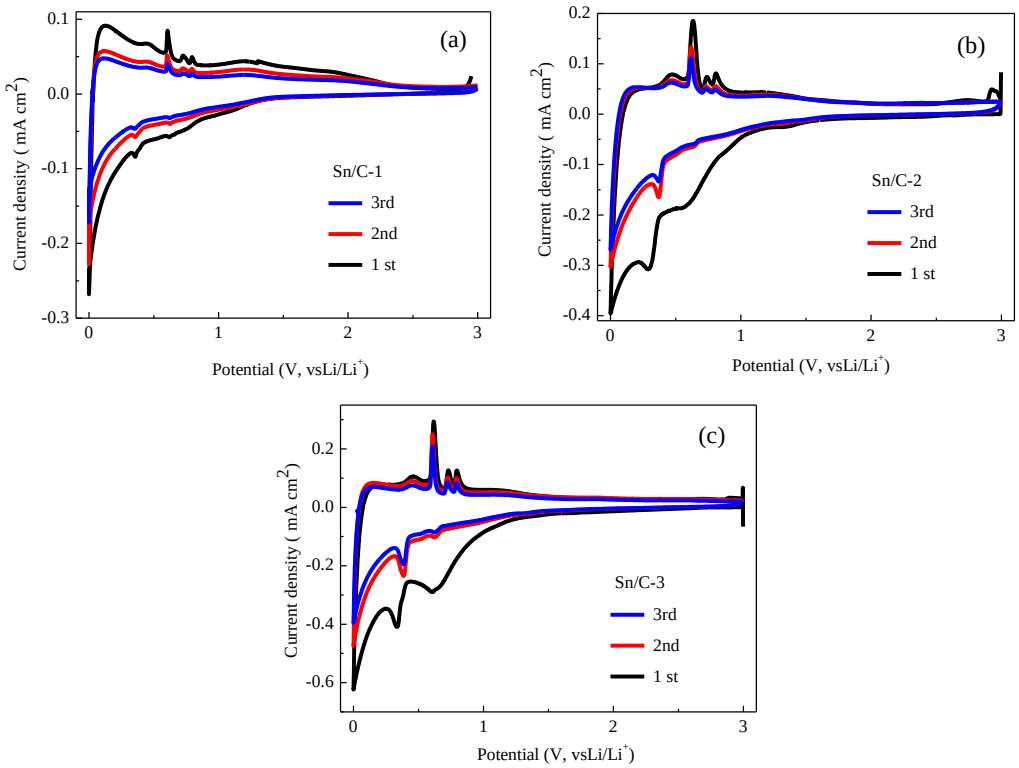

Figure 7. Cyclic voltammograms of the as-prepared samples at a scan rate of 0.1 mVs^{-1}.

4. CONCLUSIONS

In this work, Sn/C nanocomposites are prepared by a facile hydrothermal method with the size of Sn nanoparticle of about 5 nm. Such small particle size can endure the large volume expansion during lithiation-delithiation process and prevent particle pulverization. Meanwhile, carbon sheet here can prevent the aggregation of Sn nanoparticles and provides a void space for Sn nanoparticles expansion. All the Sn/C nanocomposites show good electrochemical performance especial for Sn/C-3 with Sn content of 20.9 wt%. At the current density of 200 mA g^{-1}, the initial discharge and charge capacities can up to 851.8 and 355.1 mAh g^{-1} respectively. After cycles, at the current density of 5000 mA g^{-1}, a high discharge capacity of 168.1 mAh g^{-1} can still be obtained. The high discharge capacity, excellent cycle stability and rate capacity can be attributed to the stable structure of Sn/C composite during the discharge-charge process.

ACKNOWLEDGMENTS
This work has been supported by the National Natural Science Foundation of China (21301022), the startup fund for YY from Colorado School of Mines and the Natural Science Foundation of Jiangsu Province (Grant no. BK20140256).

References

1. R. V. Noorden, *Nature*, 507 (2014) 26-28.
2. J. Cao, L. Wang, Y. Shang, M. Fang, L. Deng, J. Gao, J. Li, H. Chen, X. He, *Electrochim. Acta*, 108 (2013) 674-679.
3. S. M. Abbas, S. T. Hussain, S. Ali, N. Ahmad, N. Ali, S. Abbas, Z. Ali, *J. Solid State. Chem*, 202 (2013) 43-50.
4. X. P. Gao, H. X. Yang, *Energ. Environ. Sci*, 3 (2010) 174-189.
5. C. Wu, J. Maier, Y. Yu, *Adv. Funct. Mater*, 25 (2015) 3488-3496.
6. M. Agostinil, L. G. Rizzi, G. Cesareo, V. Russo, J. Hassoun, *Adv. Mater. Interfaces*, 2 (2015), DOI: 10.1002/admi.201500085.
7. X. Zhou, Y. Zou, J. Yang, *J. Power Sources*, 253 (2014) 287-293.
8. D. Billaud, L. Balan, R. Schneider, P. Willm, *Carbon*, 44 (2006) 2508-2515.
9. C. J. Pelliccione, E. V. Timofeeva, C. U. Segre, *J. Phys. Chem. C*, 120 (2016) 5331-5339.
10. R. Z. Hua, M. Zhu, H. Wang, J. W. Liu, O. Liu,J. Zou, *Acta Mater*, 60 (2012) 4695-4703.
11. G. Wang, Y.Q. Ma, Z.Y. Liu, J.N. Wu, *Electrochimica Acta*, 65 (2012) 275-279.
12. I.A. Courtney, J.R. Dahn, *J. Electrochem. Soc*, 144 (1997) 2045-2052.
13. L.W. Ji, Z. K. Tan, T. Kuykendall, E. J. An, Y. B. Fu, V. Battaglia, Y. G. Zhang, *Energ. Environ. Sci*, 4 (2011) 3611-3616.
14. W. B. Liu, L. Chen, C. Ye, S. C. Zhang, R. X. Lin, S. Q. Shi, *Int. J. Electrochem. Sci*, 10 (2015) 5358 - 5364.
15. X. Li, A. Dhanabalan, L. Gu, C. Wang, *Adv. Energy Mater*, 2 (2012) 238-244.
16. J. Shi, W. Shi, W. Jin, Gu. Yin, *Int. J. Electrochem. Sci*, 10 (2015) 4793-4800.
17. S. Grugeon, S. Laruelle, R. Herrera-Urbina, L. Dupont, P. Poizot, J. M. Tarascon, *J. Electrochem. Soc*, 148 (2001) A285-292.
18. J. O. Besenhard, J. Yang, M. Winter, *J. Power Sources*, 68 (1997) 87-90.
19. H. Li, L. Shi, W. Lu, X. Huang, L. Chen, *J. Electrochem. Soc*, 148 (2001) A915-922.
20. Z. Zhu, S. Wang, J. Du, Q. Jin, T, Zhang, F. Cheng, J. Chen, *Nano Lett*, 14 (2014) 153-157.
21. B. Guo, J. Shu, K. Tang, Y. Bai, Z. Wang, L. Chen, *J. Power Sources*, 177 (2008) 205-210.
22. L. Balan, R. Schneider, J. Ghanbaja, P. Willmann, D. Billaud, *Electrochim. Acta*, 51 (2006) 3385-3390.
23. J. Hassoun, G. Derrien, S. Panero, B. Scrosati, *Adv. Mater*, 20 (2008) 3169-3175.
24. X. Zhou, J.Bao, Z. Dai, Y. -G.Guo, *J. Phys. Chem. C*, 117 (2013), 25367-25373.
25. J. Qin, X. Zhang, N. Zhao, C. Shi, E. Z. Liu, J. Lia, C. He, *J. Mater. Chem. A*, 3 (2015) 23170-23179.
26. Y. Yan, L. Ben, Y. Zhan, X. Huang, *Electrochim. Acta*, 187 (2016) 186-192.
27. W. S. Chang, C. M. Park, H. J. Sohn, *J. Electroanal Chem*, 671 (2012) 67-72.
28. J. Hassoun, G. Mulas, S. Panero, B. Scrosati, *Electrochem. Commun*, 9 (2007) 2075-2081.
29. X. Hou, H. Jiang, Y. Hu, Y. Li, J. Huo, C. Li, *ACS Appl. Mater. Interfaces*, 5 (2013) 6672-6677.
30. F. Robert, F. Morato, J. Chouvin, L. Aldon, P. E. Lippens, J. O. Fourcade, J. C. Jumas, B. Simon, P. Biensan, *J. Power Sources*, 119-121 (2003) 581-584.
31. F. R. Beck, R. Epur, D. Hong, A. Manivannan, P. N. Kumta, *Electrochim. Acta*, 127 (2014) 299-306.

32. M. Marcinek, L. J. Hardwick, T. J. Richardson, X. Song, R. Kostecki, *J. Power Sources*, 173 (2007) 965-971.
33. Z. Chen, M. Zhou, Y. Cao, X. Ai, H. Yang, J. Liu, *Adv. Energy Mater*, 2 (2012) 95-102.
34. P. C. Lian, J. Y. Wang, D. D. Cai, L. X. Ding, Q. M. Jia, H. H. Wang, *Electrochim. Acta*, 116 (2014) 103-110.
35. M. Sevilla, A.B. Fuertes, *Chem. Eur. J*, 15 (2009) 4195-4203.
36. P. Lian, J. Wang, D. Cai, G. Liu, Y. Wang, H. Wang, *J. Alloys. Compd*, 604 (2014) 188-195.
37. C. Wang, Y. Li, Y. -S. Chui, Q. -H. Wu, X. Chen, W. Zhang, *Nanoscale*, 5 (2013) 10599-10604.
38. X. Huang, J. Chen, H. Yu, S. Peng, R.Cai, Q. Yan, H. H.Hng, *RSC Adv*, 3 (2013) 5310-5313.
39. D.Bresser, F. Mueller, D. Buchholz, E.Paillard, S.Passerini, *Electrochim. Acta*, 128 (2014) 163-171.
40. J. Wang, D. Li, X. Fan, L. Gou, J. Wang, Y. Li, X. Lu, Q. Li, *J. Power Sources*, 516 (2012) 33-37.
41. Y. Wang, M. Wu, Z. Jiao, J. Y. Lee, *Chem. Mater*, 21 (2009) 3210-3215.
42. Z. Li, W.Lv, C. Zhang, J. Qin, W. Wei, J. -J.Shao,D. -W. Wang, B. Li, F. Kang, Q. -H. Yang, *Nanoscale*, 6 (2014) 9554-9558.
43. H.K. Jeong, Y.P. Lee, R.J. Lahaye, M.H. Park, K.H. An, I.J. Kim, C.W. Yang,C.Y. Park, R.S. Ruoff, Y.H. Lee, *J. Am. Chem. Soc*, 130 (2008) 1362-1366.
44. X.Hou, H. Jiang, Y. Hu, Y. Li, J.Huo, C. Li, *ACS Appl. Mater. Interfaces*, 5 (2013) 6672-6677.
45. D.Ahn, X.Xiao, Y.Li, A. K.Sachdev, H. W.Park, A.Yu, Z. Chen, *J. Power Sources*, 212 (2012) 66-72.
46. D. Deng, J. Y. Lee, *Angew. Chem. Int. Ed*, 48 (2009) 1660-1663.
47. Y. H.Xu, Q.Liu, Y. J.Zhu, Y. H.Liu, A.Langrock,M. R.Zachariah, C. S. Wang, *Nano Lett*, 13 (2013) 470-474.
48. W.M.Zhang, J.S.Hu, Y.G. Guo, S.F.Zheng, L.S.Zhong, W.G.Song, L.J. Wan, *Adv. Mater*, 20 (2008) 1160-116.

© 2016 The Authors. Published by ESG (www.electrochemsci.org). This article is an open access article distributed under the terms and conditions of the Creative Commons Attribution license (http://creativecommons.org/licenses/by/4.0/).